



Measurements of charm mixing and CP violation using $D^0 \rightarrow K^\pm \pi^\mp$ decays

The LHCb collaboration[†]

Abstract

Measurements of charm mixing and CP violation parameters from the decay-time-dependent ratio of $D^0 \rightarrow K^+\pi^-$ to $D^0 \rightarrow K^-\pi^+$ decay rates and the charge-conjugate ratio are reported. The analysis uses $\bar{B} \rightarrow D^{*+}\mu^-X$, and charge-conjugate decays, where $D^{*+} \rightarrow D^0\pi^+$, and $D^0 \rightarrow K^\mp\pi^\pm$. The pp collision data are recorded by the LHCb experiment at center-of-mass energies $\sqrt{s} = 7$ and 8 TeV, corresponding to an integrated luminosity of 3 fb^{-1} . The data are analyzed under three hypotheses: (i) mixing assuming CP symmetry, (ii) mixing assuming no direct CP violation in the Cabibbo-favored or doubly Cabibbo-suppressed decay amplitudes, and (iii) mixing allowing either direct CP violation and/or CP violation in the superpositions of flavor eigenstates defining the mass eigenstates. The data are also combined with those from a previous LHCb study of $D^0 \rightarrow K\pi$ decays from a disjoint set of D^{*+} candidates produced directly in pp collisions. In all cases, the data are consistent with the hypothesis of CP symmetry.

Published in Phys. Rev. D. 95, 052004 (2017)

© CERN on behalf of the LHCb collaboration, licence CC-BY-4.0.

[†]Authors are listed at the end of this paper.

1 Introduction

The oscillation of D^0 mesons into \bar{D}^0 mesons, and vice versa, is a manifestation of the fact that the flavor and mass eigenstates of the neutral charm meson system differ. Such oscillations are also referred to as mixing. Charge-parity violation (CPV) in the superpositions of flavor eigenstates defining the mass eigenstates can lead to different mixing rates for D^0 into \bar{D}^0 and \bar{D}^0 into D^0 . The LHCb experiment has previously reported measurements of mixing and CP violation parameters from studies of $D^{*+} \rightarrow D^0\pi_s^+$, $D^0 \rightarrow K^\pm\pi^\mp$ decays, where the where the D^{*+} meson is produced directly in pp collisions [1]. In this sample, referred to as “prompt,” the flavor of the D^0 mesons at the production is determined by the charge of the slow pion π_s^+ from the strong decay of the D^{*+} meson. In this paper we extend the study using D^0 mesons produced in $\bar{B} \rightarrow D^{*+}\mu^-X$, $D^{*+} \rightarrow D^0\pi_s^+$, $D^0 \rightarrow K^\pm\pi^\mp$ and charge-conjugate decays¹, using pp collision data recorded by the LHCb experiment at center-of-mass energies $\sqrt{s} = 7$ and 8 TeV, corresponding to an integrated luminosity of 3 fb^{-1} . In this case, the flavor of the D^0 at production is tagged twice, once by the charge of the muon and once by the opposite charge of the slow pion π_s^+ produced in the D^{*+} decay, leading to very pure samples. The doubly tagged (DT) $\bar{B} \rightarrow D^{*+}\mu^-X$ candidates selected by the trigger are essentially unbiased with respect to the D^0 decay time, while those in the prompt sample are selected by the trigger with a bias towards higher decay times. As a result, the DT analysis allows for better measurements at lower decay times. In this paper, we first report the results of a mixing and CPV analysis using the DT sample, and then report the results of simultaneous fits to the DT and prompt samples.

2 Theoretical Framework

The physical eigenstates of the neutral D system, which have well-defined masses and lifetimes, can be written as linear combinations of the flavor eigenstates, which have well-defined quark content: $|D_{1,2}\rangle = p|D^0\rangle \pm q|\bar{D}^0\rangle$. We follow the convention $(CP)|D^0\rangle = -|\bar{D}^0\rangle$ [2]. The coefficients p and q are complex numbers, and satisfy the normalization condition $|p|^2 + |q|^2 = 1$. The dimensionless quantities which characterize mixing are $x = 2(m_2 - m_1)/(\Gamma_1 + \Gamma_2)$ and $y = (\Gamma_2 - \Gamma_1)/(\Gamma_1 + \Gamma_2)$, where $m_{1,2}$ and $\Gamma_{1,2}$ are the masses and widths of the mass eigenstates. In the limit of CP symmetry, p and q are equal. To the extent that CPV results only from $p \neq q$, and not from direct CPV in the D decay amplitudes themselves, and in the limit $|1 - |q/p|| \ll 1$, Wolfenstein’s superweak constraint relates the mixing and CPV parameters [3, 4]:

$$\tan \varphi = \left(1 - \left|\frac{q}{p}\right|\right) \frac{x}{y}, \quad (1)$$

where $\varphi = \arg(q/p)$. Allowing for both direct and indirect CPV , existing measurements give $x = (0.37 \pm 0.16)\%$ and $y = (0.66_{-0.10}^{+0.07})\%$ [2]. These values are consistent with Standard Model (SM) expectations for long-distance contributions [5, 6]. No evidence for CPV in mixing rates has been reported, and SM expectations are $\leq 10^{-3}$ [5–9].

We use $D^0 \rightarrow K^\pm\pi^\mp$ decays to study mixing and CPV . The decays $D^0 \rightarrow K^-\pi^+$ are called “right sign” (RS) and their decay rate is dominated by Cabibbo-favored (CF)

¹Except when otherwise explicitly stated, charge-conjugate processes are implied.

amplitudes where no direct CPV is expected in the SM or most of its extensions. Decays of $D^0 \rightarrow K^+\pi^-$ are called “wrong sign” (WS). Such decays do not have such a simple description. In the limit $(x, y) \ll 1$, an approximation of the WS decay rates of the D^0 and \bar{D}^0 mesons is

$$\begin{aligned} |\langle K^+\pi^- | H | D^0(t) \rangle|^2 &\approx \frac{e^{-\Gamma t}}{2} |\mathcal{A}_f|^2 \left\{ R_D^+ + \left| \frac{q}{p} \right| \sqrt{R_D^+} \left[y \cos(\delta - \varphi) - x \sin(\delta - \varphi) \right] (\Gamma t) \right. \\ &\quad \left. + \left| \frac{q}{p} \right|^2 \frac{x^2 + y^2}{4} (\Gamma t)^2 \right\} \end{aligned} \quad (2)$$

and

$$\begin{aligned} |\langle K^-\pi^+ | H | \bar{D}^0(t) \rangle|^2 &\approx \frac{e^{-\Gamma t}}{2} |\bar{\mathcal{A}}_f|^2 \left\{ R_D^- + \left| \frac{p}{q} \right| \sqrt{R_D^-} \left[y \cos(\delta + \varphi) - x \sin(\delta + \varphi) \right] (\Gamma t) \right. \\ &\quad \left. + \left| \frac{p}{q} \right|^2 \frac{x^2 + y^2}{4} (\Gamma t)^2 \right\}. \end{aligned} \quad (3)$$

In Eqs. (2) and (3), A_f denotes the CF transition amplitude for $D^0 \rightarrow K^-\pi^+$ and $\bar{\mathcal{A}}_f$ denotes the CF transition amplitude for $\bar{D}^0 \rightarrow K^+\pi^-$. The term Γ is the average decay width of the two mass eigenstates. Denoting the corresponding doubly Cabibbo-suppressed (DCS) amplitudes $\mathcal{A}_{\bar{f}}$ for $D^0 \rightarrow K^+\pi^-$ and $\bar{\mathcal{A}}_f$ for $\bar{D}^0 \rightarrow K^-\pi^+$, the ratios of DCS to CF amplitudes are defined to be $R_D^+ = |\mathcal{A}_{\bar{f}}/\mathcal{A}_f|^2$ and $R_D^- = |\bar{\mathcal{A}}_f/\bar{\mathcal{A}}_{\bar{f}}|^2$. The relative strong phase between the DCS and CF amplitudes $\bar{\mathcal{A}}_f$ and \mathcal{A}_f is denoted by δ . We explicitly ignore direct CPV in the phases of the CF and DCS amplitudes. As the decay time t approaches zero, the WS rate is dominated by DCS amplitudes, where no direct CPV is expected. At longer decay times, CF amplitudes associated with the corresponding antiparticle produce oscillations; by themselves, they produce a pure mixing rate proportional to $(\Gamma t)^2$, and in combination with the DCS amplitudes they produce an interference rate proportional to (Γt) . Allowing for all possible types of CPV , the time-dependent ratio of WS to RS decay rates, assuming $|x| \ll 1$ and $|y| \ll 1$, can be written as [4]

$$R(t)^\pm = R_D^\pm + \sqrt{R_D^\pm} y'^\pm \left(\frac{t}{\tau} \right) + \frac{(x'^\pm)^2 + (y'^\pm)^2}{4} \left(\frac{t}{\tau} \right)^2, \quad (4)$$

where the sign of the exponent in each term denotes whether the decay is tagged at production as D^0 (+) or as \bar{D}^0 (-). The terms x' and y' are x and y rotated by the strong phase difference δ , and $\tau = 1/\Gamma$.

The measured ratios of WS to RS decays differ from those of an ideal experiment due to matter interactions, detector response and experimental misidentifications. We use the formal approach of Ref. [1] to relate the signal ratios of Eq. (4) to a prediction of the experimentally observed ratios:

$$R(t)_{\text{pred}}^\pm = R(t)^\pm (1 - \Delta_p^\pm) (\epsilon_r)^\pm + p_{\text{other}}, \quad (5)$$

where the term $\epsilon_r \equiv \epsilon(K^+\pi^-)/\epsilon(K^-\pi^+)$ is the ratio of $K^\pm\pi^\mp$ detection efficiencies. The efficiencies related to the π_s^\pm and μ^\mp candidates explicitly cancel in this ratio. The term Δ_p^\pm describes charge-specific peaking backgrounds produced by prompt charm

mistakenly included in the DT sample, assumed to be zero after the “same-sign background subtraction” described in Sec. 4. The term p_{other} describes peaking backgrounds that contribute differently to RS and WS decays. All three of these terms are considered to be potentially time dependent.

3 Detector and Trigger

The LHCb detector [10, 11] is a single-arm forward spectrometer covering the pseudorapidity range $2 < \eta < 5$, and is designed for the study of particles containing b or c quarks. The detector includes a high-precision tracking system consisting of a silicon-strip vertex detector surrounding the pp interaction region, a large-area silicon-strip detector located upstream of a dipole magnet with a bending power of about 4 Tm, and three stations of silicon-strip detectors and straw drift tubes placed downstream of the magnet. The tracking system provides a measurement of momentum, p , of charged particles with a fractional uncertainty that varies from 0.5% at 5 GeV/ c to 1.0% at 200 GeV/ c . The minimum distance of a track to a primary vertex (PV), the impact parameter (IP), is measured with a resolution of $(15 + 29/p_T) \mu\text{m}$, where p_T is the component of the momentum transverse to the beam, in GeV/ c . Different types of charged hadrons are distinguished using information from two ring-imaging Cherenkov (RICH) detectors. Photons, electrons and hadrons are identified by a calorimeter system consisting of scintillating-pad and preshower detectors, an electromagnetic and a hadronic calorimeter. Muons are identified by a system composed of alternating layers of iron and multiwire proportional chambers.

The on-line candidate selection is performed by a trigger [12] which consists of a hardware stage, based on information from the calorimeter and muon systems, followed by a software stage. At the hardware stage, candidates are required to have a muon with $p_T > 1.64$ GeV/ c (1.76 GeV/ c) in the 2011 (2012) data sets. The software trigger, in which all charged particles with $p_T > 500$ (300) MeV/ c are reconstructed for 2011 (2012) data, first requires a muon with $p_T > 1.0$ GeV/ c , and a large χ_{IP}^2 with respect to any PV, where χ_{IP}^2 is defined as the difference in vertex fit χ^2 of a given PV reconstructed with and without the muon. Following this selection, the muon and at least one other final-state particle are required to be consistent with the topological signature of the decay of a b hadron [12]. To mitigate detector-related asymmetries, the magnet polarity is reversed periodically.

4 Off-line selection

In the off-line selection, candidates must have a muon with $p > 3$ GeV/ c , $p_T > 1.2$ GeV/ c and a track fit $\chi^2/\text{ndf} < 4$, where ndf is the number of degrees of freedom in the fit. Each of the D^0 decay products and muon candidates must have $\chi_{\text{IP}}^2 > 9$, consistent with originating from a secondary vertex. The slow pion candidate must have $p > 2$ GeV/ c and $p_T > 300$ MeV/ c , and have no associated hits in the muon stations. The combination of the K and π into a D^0 candidate must form a vertex that is well separated from the PV and have a χ^2 per degree of freedom less than 6. The D^0 candidate must also have $p_T > 1.4$ GeV/ c and its reconstructed invariant mass must lie within 24 MeV/ c^2 of its measured mass [13]. The $D^{*+}\mu^-$ invariant mass must lie in the range 3.1–5.1 GeV/ c^2 . Candidates must satisfy a vertex fit which constrains the kaon and pion to come from

the same vertex, and the muon, the slow pion and the D^0 candidate to come from a common vertex with a good χ^2/ndf . All final-state particles must pass stringent particle identification criteria from the RICH detectors, calorimeters and muon stations to improve the separation between signal and backgrounds produced by misidentified final-state particles. Candidates with reconstructed decay time $t/\tau < -0.5$ are vetoed, where τ is the measured D^0 lifetime [13] and t is calculated as $t = m_{D^0}L/p$, where L is the distance between the D^0 production and decay vertices, m_{D^0} is the observed candidate D^0 mass, and p is the D^0 momentum. The decay-time resolution is roughly 120 fs for the DT sample. Candidates which appear in both this data set and that of the earlier prompt analysis [1] are vetoed.

The same D^0 may appear in multiple candidate decay chains. In about 0.5% of cases, a single $D^0\mu^-$ combination has multiple slow pion candidates whose laboratory momentum vector directions lie within 0.6 mrad of each other. In such cases, we randomly accept one of the candidates and discard the others. When two slow pion candidates associated with a single $D^0\mu^-$ candidate are not collinear, the distributions of the $D^0\pi_s^+$ masses are consistent with the hypothesis that they (typically) result from candidates with a real D^{*+} decay plus an additional pion nearby in phase space. In such cases, we retain the multiple candidates; the fit described below correctly determines the signal and background rates as functions of $m(D^0\pi_s)$.

Real D^{*+} decays, produced either promptly or as decay products of b -hadron decays, can be mistakenly associated with muons not truly originating from b -hadron decays. In these cases, the production vertex of the D^0 may be wrongly determined. We remove these from the $D^0\pi_s^+$ distributions statistically by subtracting the corresponding $D^0\pi_s^+$ distributions of candidates where the D^{*+} and μ candidates have the same charge, the so-called same-sign samples. Signal candidates are referred to as the opposite-sign sample. The $m(D^0\pi_s^+)$ shapes to be subtracted are taken directly from the same-sign candidates, while otherwise satisfying all DT selection criteria. The absolute numbers of candidates are determined, in each bin of the D^0 decay time, by normalizing the same-sign rate to that of the opposite-sign DT sample in the $m(D^{*+}\mu^-)$ range 5.6–6 GeV/ c^2 , a region well above the masses of the B^0 and B_s^0 mesons and dominated by combinatorial backgrounds produced by false muon candidates. The ratio of same-sign to DT candidates in the signal region is roughly 1% and the ratio in the normalization region is 71%. A systematic uncertainty on the same-sign background subtraction is determined by setting the normalization factor to unity.

5 Yield extraction and fit strategy

Five bins of decay time are defined containing approximately equal numbers of RS decays. We determine D^{*+} signal yields using binned maximum likelihood fits to the $D^0\pi_s^+$ invariant mass distributions. The signal probability density function (PDF) consists of a sum of three Gaussian functions plus a Johnson S_U distribution [14] to model the asymmetric tails; the background PDFs are parametrized using empirical shapes of the form

$$(m(D^0\pi_s^+)/m_0 - 1)e^{c(m(D^0\pi_s^+)/m_0 - 1)}. \quad (6)$$

The parameter m_0 represents the kinematic limit of the distribution and is fixed to the sum of the measured mass of the pion and the D^0 [13]. The shapes of the RS and WS

$D^{*\pm}$ are assumed to be the same and to be independent of the decay time. We first fit the time-integrated RS distribution to determine signal shape parameters. These are fixed for all subsequent fits. The background parameters vary independently in each fit. Systematic uncertainties related to this choice are assessed and discussed in Sec 7. Figures 1(a) and 1(b) show the fits to the $D^0\pi_s^+$ time-integrated invariant mass distributions for RS and WS samples. They contain 1.73×10^6 and 6.68×10^3 D^{*+} decays, respectively.

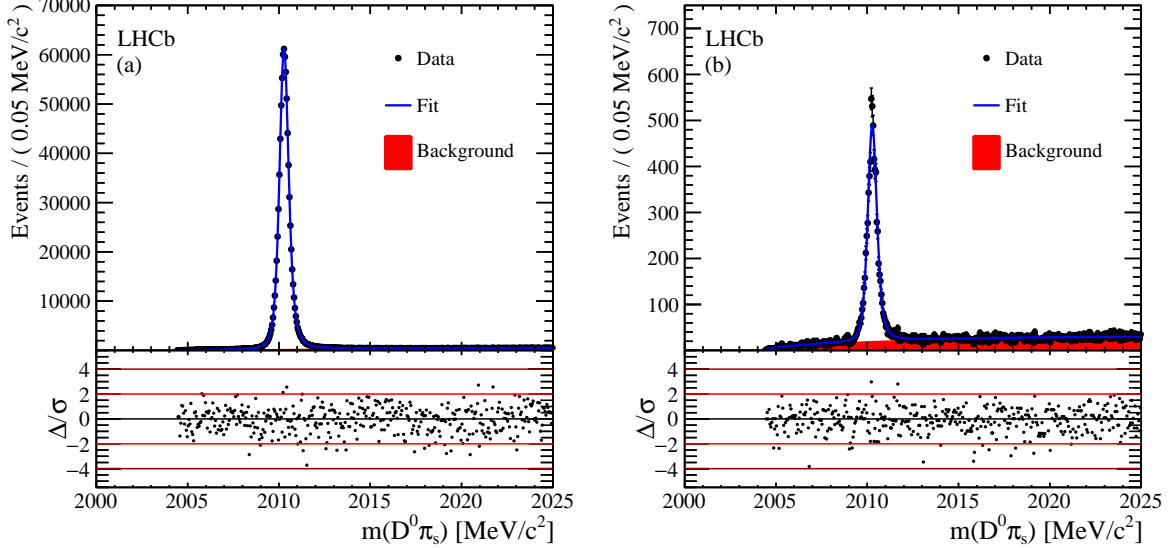


Figure 1: The time-integrated $D^0\pi_s^+$ invariant mass distributions, after same-sign subtraction, for (a) RS decays and (b) WS decays. Fit projections are overlaid. Below each plot are the normalized residual distributions.

The numbers of RS and WS signal candidates in each decay time bin are determined from fits, from which the observed WS to RS ratios are calculated. The term p_{other} is the ratio of the number of peaking events in the $m(D^0\pi_s^+)$ distribution from the D^0 sidebands of the WS sample projected into the signal region relative to the RS yield. We measure p_{other} to be $(7.4 \pm 1.8) \times 10^{-5}$. To measure the mixing and CPV parameters, the time dependence of these ratios is fit by minimizing

$$\chi^2 = \sum_i \left[\left(\frac{r_i^+ - \tilde{R}(t_i)^+}{\sigma_i^+} \right)^2 + \left(\frac{r_i^- - \tilde{R}(t_i)^-}{\sigma_i^-} \right)^2 \right] + \chi_\epsilon^2 + \chi_{\text{peaking}}^2 + \chi_{\text{other}}^2. \quad (7)$$

Here, r_i^\pm is the measured WS^\pm/RS^\pm ratio for either the $D^{*+}(D^0)$ or the $D^{*-}(\bar{D}^0)$ sample with error σ_i^\pm in a decay time bin t_i and $\tilde{R}(t_i)^\pm$ is the value of $R(t)_{\text{pred}}^\pm$ averaged over the bin. The fit accounts for uncertainties in the relative $K^\pm\pi^\mp$ tracking and reconstruction efficiencies and rates of peaking backgrounds using Gaussian constraints ($\chi_\epsilon^2 + \chi_{\text{peaking}}^2 + \chi_{\text{other}}^2$). The term χ_{other}^2 relating to the feedthrough of the prompt sample into the DT sample is explicitly zero in the DT analysis, but is needed for the simultaneous fit to the DT and prompt data sets. The statistical uncertainties reported by the fit therefore include the uncertainties associated with how precisely these factors are determined.

Three fits are performed using this framework. First, we fit the data assuming CP symmetry in the formalism of Eq. (4) [*i.e.* $R^+ = R^-$, $(x'^+)^2 = (x'^-)^2$ and $y'^+ = y'^-$]. Second, we fit the data requiring CP symmetry in the CF and DCS amplitudes (*i.e.* $R^+ = R^-$), but allow CPV in the mixing parameters themselves [$(x'^{\pm})^2$ and y'^{\pm}]. Finally, we fit the data allowing all the parameters to float freely.

6 Relative efficiencies

The relative efficiency ϵ_r , used in Eq. (5), accounts for instrumental asymmetries in the $K^{\mp}\pi^{\pm}$ reconstruction efficiencies. The largest source of these is the difference between the inelastic cross sections of K^- and π^- mesons with matter, and those of their antiparticles. We measure ϵ_r , accounting for all detector effects as well as cross-section differences in a similar manner to the prompt analysis [1]. The efficiency is determined using the product of $D^+ \rightarrow K^- \pi^+ \pi^+$ and $D^+ \rightarrow K_s^0 (\rightarrow \pi^+ \pi^-) \pi^+$ decay yields divided by the product of the corresponding charge-conjugate decay yields. The expected CPV associated with differing $K^0 \rightarrow K_s^0$ and $\bar{K}^0 \rightarrow K_s^0$ rates and the differences in neutral kaon inelastic cross-sections with matter are accounted for [15]. Trigger and detection asymmetries associated with the muon candidates are calculated directly from data and included in the determination. The 1% asymmetry between D^+ and D^- production rates [16] cancels in this ratio, provided that the kinematic distributions are consistent across samples. To ensure this cancellation, we weight the $D^+ \rightarrow K^- \pi^+ \pi^+$ candidates such that the kaon p_T and η and pion p_T distributions match those in the DT $K\pi$ sample. Similarly, $D^+ \rightarrow K_s^0 \pi^+$ candidates are weighted by D^+ p_T and η and pion p_T distributions to match those of the $D^+ \rightarrow K^- \pi^+ \pi^+$. The weighting is performed using a gradient boosted decision tree implemented in SCIKIT-LEARN [17] accessed using the HEP_ML framework [18]. We measure the $K\pi$ detection asymmetry to be $A(K\pi) = (\epsilon_r - 1)/(\epsilon_r + 1) = (0.90 \pm 0.18 \pm 0.10)\%$ for the sample of this analysis, and find it to be independent of decay time.

7 Systematic uncertainties

The systematic uncertainties of the DT analysis are summarized in Table 1. To avoid bias, offsets to each WS/RS ratio were randomly chosen to blind both direct and indirect CPV , as well as the central values of the mixing parameters. Cross-checks of the blinded data were performed by splitting the data into disjoint subsamples according to criteria that might be sensitive to systematic variations in detector response. We considered two subsamples of magnet polarity, integrated over the entire data taking period, two subsamples for the year in which the data was recorded, four subsamples splitting according to magnet polarity and year of data acquisition, three subsamples each of K^{\pm} momentum, μ^{\pm} transverse momentum and π^{\pm} transverse momentum. All observed variations in the fit results are consistent with being statistical fluctuations.

The ratio of RS D^{*-} to RS D^{*+} decays as a function of decay time is consistent with the hypothesis of decay-time independence with a p value of 0.06. We conservatively estimate a systematic uncertainty by modifying ϵ_r to allow for a linear time dependence that gives the best description of the RS data. As seen in Table 1, this has essentially no effect on the results of the mixing fit where CP symmetry is assumed to be exact. It is the dominant systematic uncertainty in the fit requiring $R_D^+ = R_D^-$, and it produces a

Table 1: Summary of systematic uncertainties for the DT analysis for each of the three fits described in the text.

Source of systematic uncertainty	Uncertainty on parameter					
	No <i>CPV</i>					
	$R_D[10^{-3}]$	$y'[10^{-3}]$	$x'^2[10^{-4}]$			
$D^{*+}\mu^+$ scaling	0.01	0.04	0.04			
$A(K\pi)$ time dependence	0.01	0.07	0.04			
RS fit model time variation	0.00	0.01	0.03			
No prompt veto	0.01	0.16	0.09			
Total	0.01	0.18	0.11			
	No direct <i>CPV</i>					
	$R_D[10^{-3}]$	$y'^+[10^{-3}]$	$(x'^+)^2[10^{-4}]$	$y'^-[10^{-3}]$	$(x'^-)^2[10^{-4}]$	
$D^{*+}\mu^+$ scaling	0.01	0.04	0.04	0.03	0.04	
$A(K\pi)$ time dependence	0.01	1.17	0.98	1.64	1.67	
RS fit model time variation	0.00	0.02	0.03	0.01	0.03	
No prompt veto	0.01	0.11	0.00	0.19	0.19	
Total	0.01	1.17	0.98	1.66	1.68	
	All <i>CPV</i> allowed					
	$R_D^+[10^{-3}]$	$y'^+[10^{-3}]$	$(x'^+)^2[10^{-4}]$	$R_D^-[10^{-3}]$	$y'^-[10^{-3}]$	$(x'^-)^2[10^{-4}]$
$D^{*+}\mu^+$ scaling	0.01	0.03	0.04	0.01	0.04	0.04
$A(K\pi)$ time dependence	0.06	0.25	0.03	0.07	0.28	0.03
RS fit model time variation	0.00	0.01	0.01	0.00	0.04	0.05
No prompt veto	0.01	0.09	0.01	0.01	0.21	0.19
Potential fit biases	0.00	0.18	0.30	0.00	0.18	0.33
Total	0.06	0.32	0.31	0.07	0.40	0.38

systematic uncertainty much smaller than the statistical error in the fit that allows all forms of *CPV*. Uncertainties are not symmetrized.

We determine systematic uncertainties related to variations of the fit procedure by considering alternative choices. To determine uncertainties related to subtraction of the same-sign background $m(D^0\pi_s)$ distributions from the opposite-sign ones, we subtract the raw same-sign distributions rather than the scaled distributions. To determine uncertainties related to excluding candidates considered in the prompt analysis [1] from the DT analysis, we repeat the DT analysis including those candidates. As an alternative to using a single signal shape at all decay times, we determine signal shapes using the RS signal in each decay time bin. We evaluate potential biases in fitting procedure by generating and fitting 11,000 simulated DT samples with values of x and y spanning the 2σ contour about the average values reported by HFAG [2]. The biases we observe are nonzero, and appear to be independent of the generated values. We assign a systematic uncertainty equal to the full observed bias. Table 1 summarizes the results of these studies. All systematic uncertainties are propagated to the final results using their full covariance matrices.

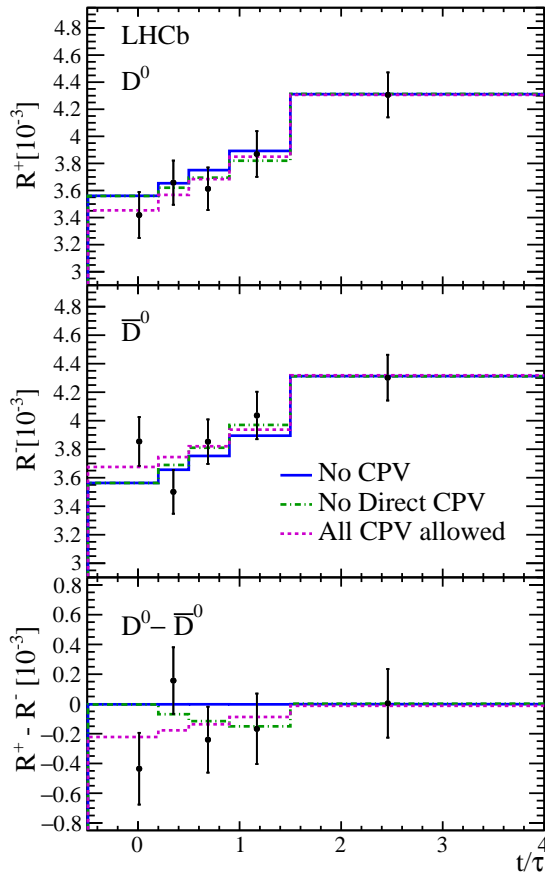


Figure 2: Efficiency corrected and SS background subtracted ratios of WS/RS decays and fit projections for the DT sample. The top plot shows the D^0 ($R^+(t)$) sample. The middle plot shows the \bar{D}^0 ($R^-(t)$) sample. The bottom plot shows the difference between the top and middle plots. In all cases, the error bars superposed on the data points are those from the χ^2 minimization fits with no accounting for additional systematic uncertainties. The projections shown are for fits assuming CP symmetry (solid blue line), allowing no direct CPV (dashed-dotted green line), and allowing all forms of CPV (dashed magenta line). Bins are centered at the average value of t/τ of the bin.

8 Results

The efficiency-corrected and same-sign (SS) background subtracted WS/RS ratios of the DT data and the three fits described earlier are shown in Fig. 2. The fits are shown in a binned projection. The top two plots show the WS/RS ratio as a function of decay time for the candidates tagged at production as D^0 [$R^+(t)$] and as \bar{D}^0 [$R^-(t)$]. Both sets of points appear to lie on straight lines that intersect the vertical axis near 3.5×10^{-3} at $t/\tau = 0$ and rise approximately linearly to 4.3×10^{-3} near $t/\tau = 2.5$. The difference between the two ratios is shown in the bottom plot. The fit values for the parameters and their uncertainties, are collected in Table 2. The data are clearly consistent with the hypothesis of CP symmetry, *i.e.* that the two samples share exactly the same mixing parameters. If direct CPV is assumed to be zero ($R^+ = R^-$ at $t/\tau = 0$), as expected if tree-level amplitudes dominate the CF and DCS amplitudes, the difference in mixing rates

(the slope) is observed to be very small. For this data set, the statistical uncertainties are all much greater than the corresponding systematic uncertainties, which include the uncertainties from ϵ_r and peaking backgrounds. Correlation matrices between the fitted parameters are included in Appendix A, Tables 5–7.

Table 2: Fitted parameters of the DT sample. The first uncertainties include the statistical uncertainty, as well as the peaking backgrounds and the $K\pi$ detection efficiency, and the second are systematic.

Parameter	Value
No CPV	
$R_D[10^{-3}]$	$3.48 \pm 0.10 \pm 0.01$
$x'^2[10^{-4}]$	$0.28 \pm 3.10 \pm 0.11$
$y'[10^{-3}]$	$4.60 \pm 3.70 \pm 0.18$
χ^2/ndf	$6.3/7$
No direct CPV	
$R_D[10^{-3}]$	$3.48 \pm 0.10 \pm 0.01$
$(x'^+)^2 [10^{-4}]$	$1.94 \pm 3.67 \pm 0.98$
$y'^+[10^{-3}]$	$2.79 \pm 4.27 \pm 1.17$
$(x'^-)^2 [10^{-4}]$	$-1.53 \pm 4.04 \pm 1.68$
$y'^-[10^{-3}]$	$6.51 \pm 4.38 \pm 1.66$
χ^2/ndf	$5.6/5$
All CPV allowed	
$R_D^+[10^{-3}]$	$3.38 \pm 0.15 \pm 0.06$
$(x'^+)^2 [10^{-4}]$	$-0.19 \pm 4.46 \pm 0.31$
$y'^+[10^{-3}]$	$5.81 \pm 5.25 \pm 0.32$
$R_D^-[10^{-3}]$	$3.60 \pm 0.15 \pm 0.07$
$(x'^-)^2 [10^{-4}]$	$0.79 \pm 4.31 \pm 0.38$
$y'^-[10^{-3}]$	$3.32 \pm 5.21 \pm 0.40$
χ^2/ndf	$4.5/4$

The data of the prompt analysis [1], those of the DT analysis and the results of fitting the two (disjoint) samples simultaneously are shown in Fig. 3. The combined sets of data points in the top and middle plots lie on slightly curved lines that intersect the vertical axis near 3.4×10^{-3} at $t/\tau = 0$ and rise to approximately 5.9×10^{-3} just above $t/\tau = 6.0$. The samples are consistent with CP symmetry. The results of the simultaneous fit are reported in Table 3. The corresponding results from the prompt analysis [1] are also reported in Table 3 for comparison. In Table 3, the statistical and systematic uncertainties have been added in quadrature to allow direct comparison of the two sets of results. As all the systematic uncertainties for the prompt analysis were evaluated using χ^2 constraints as in Eq. (7), we determine systematic uncertainties for the simultaneous fits by repeating

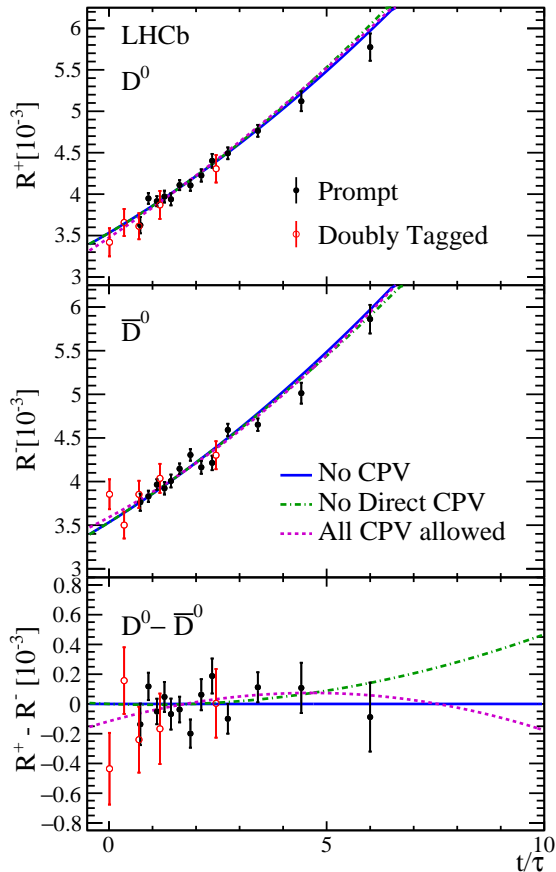


Figure 3: Efficiency-corrected data and fit projections for the DT (red open circles) and prompt (black filled circles) samples. The top plot shows the D^0 ($R^+(t)$) samples. The middle plot shows the \bar{D}^0 ($R^-(t)$) samples. The bottom plot shows the difference between the top and middle plots. In all cases, the error bars superposed on the data points are those from the χ^2 minimization fits without accounting for additional systematic uncertainties. The projections shown are for fits assuming CP symmetry (solid blue line), allowing no direct CPV (dashed-dotted green line), and allowing all forms of CPV (dashed magenta line). Bins are centered at the average t/τ of the bin.

the fit variations as for the DT fit. These systematics are reported in Table 4. In general, the uncertainties from the combined fits are 10%–20% lower than those from the previous measurement [1]. The decrease in the uncertainty comes from the improved precision that the DT sample provides at low D^0 decay time. The corresponding correlation matrices are given in Appendix B, Tables 8–10.

The combined fit of the DT and prompt sample is consistent with CP symmetry. The WS D^0 and \bar{D}^0 rates at $t/\tau = 0$ are equal within experimental uncertainties, indicating no direct CP violation. Similarly, the mixing rates are consistent within experimental uncertainties, as seen in the bottom plot of Fig. 3. In the combined fit of this analysis, assuming no direct CP violation, the difference between the projected WS/RS rates at $t/\tau = 6.0$ is only 0.15×10^{-3} (see the dashed-dotted line in the bottom plot of Fig. 3), where the WS/RS rates themselves have increased by about 2.5×10^{-3} (see the top and middle plots).

The determination of the CPV parameters $|q/p|$ and φ from the difference in rates of WS D^0 and \bar{D}^0 requires the use of independent measurements, as these variables appear in the WS/RS ratios only in combination with the strong phase difference δ and with x and y , as seen in Eqs. (2) and (3). When the results are combined with independent measurements, as done by the Heavy Flavor Averaging Group [2], the precision of the constraints on $|q/p| - 1$ approximately scale with the precision of the difference in WS/RS ratios at high decay time divided by the average increase. Utilizing theoretical constraints such as Eq. (1), in addition to the experimental data, the precision on $|q/p|$ improves by about a factor of 4 [2].

9 Summary

In summary, the analysis of mixing and CPV parameters using the DT $D^0 \rightarrow K^\mp \pi^\pm$ samples provides results consistent with those of our earlier prompt analysis. Simultaneously fitting the disjoint data sets of the two analyses improves the precision of the measured parameters by 10%–20%, even though the DT analysis is based on almost 40 times fewer candidates than the prompt analysis. In part, this results from much cleaner signals in the DT analysis, and, in part, it results from the complementary higher acceptance of the DT trigger at low D decay times. The current results supersede those of our earlier publication [1].

Table 3: Simultaneous fit result of the DT and prompt samples. The prompt-only results from [1] are shown on the right for comparison. Statistical and systematic errors have been added in quadrature.

Parameter	DT + Prompt	Prompt-only
<i>No CPV</i>		
$R_D[10^{-3}]$	3.533 ± 0.054	3.568 ± 0.067
$x'^2[10^{-4}]$	0.36 ± 0.43	0.55 ± 0.49
$y'[10^{-3}]$	5.23 ± 0.84	4.8 ± 0.9
χ^2/ndf	96.6/111	86.4/101
<i>No direct CPV</i>		
$R_D[10^{-3}]$	3.533 ± 0.054	3.568 ± 0.067
$(x'^+)^2 [10^{-4}]$	0.49 ± 0.50	0.64 ± 0.56
$y'^+[10^{-3}]$	5.14 ± 0.91	4.8 ± 1.1
$(x'^-)^2 [10^{-4}]$	0.24 ± 0.50	0.46 ± 0.55
$y'^-[10^{-3}]$	5.32 ± 0.91	4.8 ± 1.1
χ^2/ndf	96.1/109	86.0/99
<i>All CPV allowed</i>		
$R_D^+[10^{-3}]$	3.474 ± 0.081	3.545 ± 0.095
$(x'^+)^2 [10^{-4}]$	0.11 ± 0.65	0.49 ± 0.70
$y'^+[10^{-3}]$	5.97 ± 1.25	5.1 ± 1.4
$R_D^-[10^{-3}]$	3.591 ± 0.081	3.591 ± 0.090
$(x'^-)^2 [10^{-4}]$	0.61 ± 0.61	0.60 ± 0.68
$y'^-[10^{-3}]$	4.50 ± 1.21	4.5 ± 1.4
χ^2/ndf	95.0/108	85.9/98

Table 4: Systematic uncertainties for the simultaneous fits of the DT and prompt datasets.

Systematic uncertainty	Uncertainty on parameter					
	No <i>CPV</i>					
	$R_D[10^{-3}]$	$y'[10^{-3}]$	$x'^2[10^{-4}]$			
$D^{*+}\mu^+$ scaling	0.00	0.05	0.02			
$A(K\pi)$ time dependence	0.00	0.02	0.01			
RS fit model time variation	0.00	0.00	0.00			
No prompt veto	0.00	0.04	0.02			
Total	0.01	0.07	0.03			
	No direct <i>CPV</i>					
	$R_D[10^{-3}]$	$y'^+[10^{-3}]$	$(x'^+)^2[10^{-4}]$	$y'^-[10^{-3}]$	$(x'^-)^2[10^{-4}]$	
$D^{*+}\mu^+$ scaling	0.00	0.05	0.02	0.05	0.02	
$A(K\pi)$ time dependence	0.00	0.02	0.02	0.06	0.03	
RS fit model time variation	0.00	0.00	0.00	0.00	0.00	
No prompt veto	0.00	0.04	0.02	0.04	0.02	
Total	0.01	0.07	0.03	0.09	0.05	
	All <i>CPV</i> allowed					
	$R_D^+[10^{-3}]$	$y'^+[10^{-3}]$	$(x'^+)^2[10^{-4}]$	$R_D^-[10^{-3}]$	$y'^-[10^{-3}]$	$(x'^-)^2[10^{-4}]$
$D^{*+}\mu^+$ scaling	0.00	0.06	0.02	0.00	0.05	0.02
$A(K\pi)$ time dependence	0.03	0.33	0.15	0.03	0.31	0.13
RS fit model time variation	0.00	0.00	0.00	0.00	0.01	0.00
No prompt veto	0.00	0.05	0.02	0.00	0.03	0.01
Total	0.03	0.34	0.15	0.03	0.31	0.13

Acknowledgements

We express our gratitude to our colleagues in the CERN accelerator departments for the excellent performance of the LHC. We thank the technical and administrative staff at the LHCb institutes. We acknowledge support from CERN and from the national agencies: CAPES, CNPq, FAPERJ and FINEP (Brazil); NSFC (China); CNRS/IN2P3 (France); BMBF, DFG and MPG (Germany); INFN (Italy); FOM and NWO (Netherlands); MNiSW and NCN (Poland); MEN/IFA (Romania); MinES and FASO (Russia); MinECo (Spain); SNSF and SER (Switzerland); NASU (Ukraine); STFC (United Kingdom); and NSF (USA). We acknowledge the computing resources that are provided by CERN, IN2P3 (France), KIT and DESY (Germany), INFN (Italy), SURF (Netherlands), PIC (Spain), GridPP (United Kingdom), RRCKI and Yandex LLC (Russia), CSCS (Switzerland), IFIN-HH (Romania), CBPF (Brazil), PL-GRID (Poland) and OSC (USA). We are indebted to the communities behind the multiple open source software packages on which we depend. Individual groups or members have received support from AvH Foundation (Germany), EPLANET, Marie Skłodowska-Curie Actions and ERC (European Union), Conseil Général de Haute-Savoie, Labex ENIGMASS and OCEVU, Région Auvergne (France), RFBR and Yandex LLC (Russia), GVA, XuntaGal and GENCAT (Spain), Herchel Smith Fund, The Royal Society, Royal Commission for the Exhibition of 1851 and the Leverhulme Trust (United Kingdom).

Appendices

A Correlation matrices of the DT Fit

Table 5: Correlation matrix for the no CPV fit to the DT data.

	R_D	y'	x'^2
R_D	1	-0.678	0.607
y'		1	-0.941
x'^2			1

Table 6: Correlation matrix for the no direct CPV fit to the DT data.

	R_D	y'^+	$(x'^+)^2$	y'^-	$(x'^-)^2$
R_D	1	-0.369	0.261	-0.374	0.309
y'^+		1	-0.944	0.448	-0.370
$(x'^+)^2$			1	-0.352	0.290
y'^-				1	-0.967
$(x'^-)^2$					1

Table 7: Correlation matrix for the all CPV allowed fit to the DT data.

	R_D^+	y'^+	$(x'^+)^2$	R_D^-	y'^-	$(x'^-)^2$
R_D^+	1	-0.658	0.043	-0.005	0.000	0.000
y'^+		1	0.438	-0.001	-0.000	-0.001
$(x'^+)^2$			1	-0.000	-0.000	-0.002
R_D^-				1	-0.621	0.074
y'^-					1	0.050
$(x'^-)^2$						1

B Correlation matrices of the DT + Prompt Fit

Table 8: Correlation matrix for the no CPV simultaneous fit to the prompt + DT data sets.

	R_D	y'	x'^2
R_D	1	-0.932	0.826
y'		1	-0.959
x'^2			1

Table 9: Correlation matrix for the no direct CPV simultaneous fit to the prompt + DT data sets.

	R_D	y'^+	$(x'^+)^2$	y'^-	$(x'^-)^2$
R_D	1	-0.854	0.686	-0.751	0.586
y'^+		1	-0.925	0.631	-0.501
$(x'^+)^2$			1	-0.563	0.458
y'^-				1	-0.937
$(x'^-)^2$					1

Table 10: Correlation matrix for the all CPV allowed simultaneous fit to the prompt + DT data sets.

	R_D^+	y'^+	$(x'^+)^2$	R_D^-	y'^-	$(x'^-)^2$
R_D^+	1	-0.920	0.823	-0.007	-0.010	0.008
y'^+		1	-0.962	-0.011	0.000	-0.002
$(x'^+)^2$			1	0.009	-0.002	0.004
R_D^-				1	-0.918	0.812
y'^-					1	-0.956
$(x'^-)^2$						1

References

- [1] LHCb collaboration, R. Aaij *et al.*, *Measurement of D^0 - \bar{D}^0 mixing parameters and search for CP violation using $D^0 \rightarrow K^+\pi^-$ decays*, Phys. Rev. Lett. **111** (2013) 251801, arXiv:1309.6534.
- [2] Heavy Flavor Averaging Group, Y. Amhis *et al.*, *Averages of b-hadron, c-hadron, and τ -lepton properties as of summer 2014*, arXiv:1412.7515, updated results and plots available at <http://www.slac.stanford.edu/xorg/hfag/>. Accessed on 11 November, 2016.
- [3] L. Wolfenstein, *Violation of CP invariance and the possibility of very weak interactions*, Phys. Rev. Lett. **13** (1964) 562.
- [4] A. L. Kagan and M. D. Sokoloff, *On indirect CP violation and implications for $D^0 - \bar{D}^0$ and $B_s^0 - \bar{B}_s^0$ mixing*, Phys. Rev. **D80** (2009) 076008, arXiv:0907.3917.
- [5] A. F. Falk *et al.*, *$D^0 - \bar{D}^0$ mass difference from a dispersion relation*, Phys. Rev. **D69** (2004) 114021.
- [6] J. F. Donoghue, E. Golowich, B. R. Holstein, and J. Trampetić, *Dispersive effects in $D^0 - \bar{D}^0$ mixing*, Phys. Rev. **D33** (1986) 179.
- [7] A. F. Falk, Y. Grossman, Z. Ligeti, and A. A. Petrov, *SU(3) breaking and $D^0 - \bar{D}^0$ mixing*, Phys. Rev. **D65** (2002) 054034.
- [8] S. Bianco, F. L. Fabbri, D. Benson, and I. Bigi, *A Cicerone for the physics of charm*, Riv. Nuovo Cim. **26N7** (2003) 1, arXiv:hep-ex/0309021.
- [9] G. Burdman and I. Shipsey, *$D^0 - \bar{D}^0$ mixing and rare charm decays*, Ann. Rev. Nucl. Part. Sci. **53** (2003) 431, arXiv:hep-ph/0310076.
- [10] LHCb collaboration, A. A. Alves Jr. *et al.*, *The LHCb detector at the LHC*, JINST **3** (2008) S08005.
- [11] LHCb collaboration, R. Aaij *et al.*, *LHCb detector performance*, Int. J. Mod. Phys. **A30** (2015) 1530022, arXiv:1412.6352.
- [12] R. Aaij *et al.*, *The LHCb trigger and its performance in 2011*, JINST **8** (2013) P04022, arXiv:1211.3055.
- [13] Particle Data Group, K. A. Olive *et al.*, *Review of particle physics*, Chin. Phys. **C38** (2014) 090001, and 2015 update.
- [14] N. L. Johnson, *Systems of frequency curves generated by methods of translation*, Biometrika **36** (1949) 149.
- [15] LHCb collaboration, R. Aaij *et al.*, *Measurement of CP asymmetry in $D^0 \rightarrow K^-K^+$ and $D^0 \rightarrow \pi^-\pi^+$ decays*, JHEP **07** (2014) 041, arXiv:1405.2797.
- [16] LHCb collaboration, R. Aaij *et al.*, *Measurement of the D^\pm production asymmetry in 7 TeV pp collisions*, Phys. Lett. **B718** (2013) 902, arXiv:1210.4112.

- [17] F. Pedregosa *et al.*, *Scikit-learn: Machine Learning in Python*, J. Machine Learning Res. **12** (2011) 2825, [arXiv:1201.0490](https://arxiv.org/abs/1201.0490).
- [18] A. Rogozhnikov *et al.*, *hep_ml*, https://arogozhnikov.github.io/hep_ml/.

LHCb collaboration

R. Aaij⁴⁰, B. Adeva³⁹, M. Adinolfi⁴⁸, Z. Ajaltouni⁵, S. Akar⁶, J. Albrecht¹⁰, F. Alessio⁴⁰, M. Alexander⁵³, S. Ali⁴³, G. Alkhazov³¹, P. Alvarez Cartelle⁵⁵, A.A. Alves Jr⁵⁹, S. Amato², S. Amerio²³, Y. Amhis⁷, L. An⁴¹, L. Anderlini¹⁸, G. Andreassi⁴¹, M. Andreotti^{17,g}, J.E. Andrews⁶⁰, R.B. Appleby⁵⁶, F. Archilli⁴³, P. d'Argent¹², J. Arnau Romeu⁶, A. Artamonov³⁷, M. Artuso⁶¹, E. Aslanides⁶, G. Auriemma²⁶, M. Baalouch⁵, I. Babuschkin⁵⁶, S. Bachmann¹², J.J. Back⁵⁰, A. Badalov³⁸, C. Baesso⁶², S. Baker⁵⁵, W. Baldini¹⁷, R.J. Barlow⁵⁶, C. Barschel⁴⁰, S. Barsuk⁷, W. Barter⁴⁰, M. Baszczyk²⁷, V. Batozskaya²⁹, B. Batsukh⁶¹, V. Battista⁴¹, A. Bay⁴¹, L. Beaucourt⁴, J. Beddow⁵³, F. Bedeschi²⁴, I. Bediaga¹, L.J. Bel⁴³, V. Bellee⁴¹, N. Belloli^{21,i}, K. Belous³⁷, I. Belyaev³², E. Ben-Haim⁸, G. Bencivenni¹⁹, S. Benson⁴³, J. Benton⁴⁸, A. Berezhnoy³³, R. Bernet⁴², A. Bertolin²³, F. Betti¹⁵, M.-O. Bettler⁴⁰, M. van Beuzekom⁴³, I. Bezshyiko⁴², S. Bifani⁴⁷, P. Billoir⁸, T. Bird⁵⁶, A. Birnkraut¹⁰, A. Bitadze⁵⁶, A. Bizzeti^{18,u}, T. Blake⁵⁰, F. Blanc⁴¹, J. Blouw^{11,†}, S. Blusk⁶¹, V. Bocci²⁶, T. Boettcher⁵⁸, A. Bondar^{36,w}, N. Bondar^{31,40}, W. Bonivento¹⁶, A. Borgheresi^{21,i}, S. Borghi⁵⁶, M. Borisyak³⁵, M. Borsato³⁹, F. Bossu⁷, M. Boubdir⁹, T.J.V. Bowcock⁵⁴, E. Bowen⁴², C. Bozzi^{17,40}, S. Braun¹², M. Britsch¹², T. Britton⁶¹, J. Brodzicka⁵⁶, E. Buchanan⁴⁸, C. Burr⁵⁶, A. Bursche², J. Buytaert⁴⁰, S. Cadeddu¹⁶, R. Calabrese^{17,g}, M. Calvi^{21,i}, M. Calvo Gomez^{38,m}, A. Camboni³⁸, P. Campana¹⁹, D. Campora Perez⁴⁰, D.H. Campora Perez⁴⁰, L. Capriotti⁵⁶, A. Carbone^{15,e}, G. Carboni^{25,j}, R. Cardinale^{20,h}, A. Cardini¹⁶, P. Carniti^{21,i}, L. Carson⁵², K. Carvalho Akiba², G. Casse⁵⁴, L. Cassina^{21,i}, L. Castillo Garcia⁴¹, M. Cattaneo⁴⁰, Ch. Cauet¹⁰, G. Cavallero²⁰, R. Cenci^{24,t}, M. Charles⁸, Ph. Charpentier⁴⁰, G. Chatzikonstantinidis⁴⁷, M. Chefdeville⁴, S. Chen⁵⁶, S.-F. Cheung⁵⁷, V. Chobanova³⁹, M. Chrzaszcz^{42,27}, X. Cid Vidal³⁹, G. Ciezarek⁴³, P.E.L. Clarke⁵², M. Clemencic⁴⁰, H.V. Cliff⁴⁹, J. Closier⁴⁰, V. Coco⁵⁹, J. Cogan⁶, E. Cogneras⁵, V. Cogoni^{16,40,f}, L. Cojocariu³⁰, G. Collazuol^{23,o}, P. Collins⁴⁰, A. Comerma-Montells¹², A. Contu⁴⁰, A. Cook⁴⁸, G. Coombs⁴⁰, S. Coquereau³⁸, G. Corti⁴⁰, M. Corvo^{17,g}, C.M. Costa Sobral⁵⁰, B. Couturier⁴⁰, G.A. Cowan⁵², D.C. Craik⁵², A. Crocombe⁵⁰, M. Cruz Torres⁶², S. Cunliffe⁵⁵, R. Currie⁵⁵, C. D'Ambrosio⁴⁰, F. Da Cunha Marinho², E. Dall'Occo⁴³, J. Dalseno⁴⁸, P.N.Y. David⁴³, A. Davis⁵⁹, O. De Aguiar Francisco², K. De Bruyn⁶, S. De Capua⁵⁶, M. De Cian¹², J.M. De Miranda¹, L. De Paula², M. De Serio^{14,d}, P. De Simone¹⁹, C.-T. Dean⁵³, D. Decamp⁴, M. Deckenhoff¹⁰, L. Del Buono⁸, M. Demmer¹⁰, D. Derkach³⁵, O. Deschamps⁵, F. Dettori⁴⁰, B. Dey²², A. Di Canto⁴⁰, H. Dijkstra⁴⁰, F. Dordei⁴⁰, M. Dorigo⁴¹, A. Dosil Suárez³⁹, A. Dovbnya⁴⁵, K. Dreimanis⁵⁴, L. Dufour⁴³, G. Dujany⁵⁶, K. Dungs⁴⁰, P. Durante⁴⁰, R. Dzhelyadin³⁷, A. Dziurda⁴⁰, A. Dzyuba³¹, N. Deléage⁴, S. Easo⁵¹, M. Ebert⁵², U. Egede⁵⁵, V. Egorychev³², S. Eidelman^{36,w}, S. Eisenhardt⁵², U. Eitschberger¹⁰, R. Ekelhof¹⁰, L. Eklund⁵³, Ch. Elsasser⁴², S. Ely⁶¹, S. Esen¹², H.M. Evans⁴⁹, T. Evans⁵⁷, A. Falabella¹⁵, N. Farley⁴⁷, S. Farry⁵⁴, R. Fay⁵⁴, D. Fazzini^{21,i}, D. Ferguson⁵², V. Fernandez Albor³⁹, A. Fernandez Prieto³⁹, F. Ferrari^{15,40}, F. Ferreira Rodrigues¹, M. Ferro-Luzzi⁴⁰, S. Filippov³⁴, R.A. Fini¹⁴, M. Fiore^{17,g}, M. Fiorini^{17,g}, M. Firlej²⁸, C. Fitzpatrick⁴¹, T. Fiutowski²⁸, F. Fleuret^{7,b}, K. Fohl⁴⁰, M. Fontana^{16,40}, F. Fontanelli^{20,h}, D.C. Forshaw⁶¹, R. Forty⁴⁰, V. Franco Lima⁵⁴, M. Frank⁴⁰, C. Frei⁴⁰, J. Fu^{22,q}, E. Furfaro^{25,j}, C. Färber⁴⁰, A. Gallas Torreira³⁹, D. Galli^{15,e}, S. Gallorini²³, S. Gambetta⁵², M. Gandelman², P. Gandini⁵⁷, Y. Gao³, L.M. Garcia Martin⁶⁸, J. García Pardiñas³⁹, J. Garra Tico⁴⁹, L. Garrido³⁸, P.J. Garsed⁴⁹, D. Gascon³⁸, C. Gaspar⁴⁰, L. Gavardi¹⁰, G. Gazzoni⁵, D. Gerick¹², E. Gersabeck¹², M. Gersabeck⁵⁶, T. Gershon⁵⁰, Ph. Ghez⁴, S. Giani⁴¹, V. Gibson⁴⁹, O.G. Girard⁴¹, L. Giubega³⁰, K. Gizdov⁵², V.V. Gligorov⁸, D. Golubkov³², A. Golutvin^{55,40}, A. Gomes^{1,a}, I.V. Gorelov³³, C. Gotti^{21,i}, M. Grabalosa Gándara⁵, R. Graciani Diaz³⁸, L.A. Granado Cardoso⁴⁰, E. Graugés³⁸, E. Graverini⁴², G. Graziani¹⁸, A. Greco³⁰, P. Griffith⁴⁷, L. Grillo^{21,40,i}, B.R. Gruberg Cazon⁵⁷, O. Grünberg⁶⁶, E. Gushchin³⁴, Yu. Guz³⁷, T. Gys⁴⁰,

C. Göbel⁶², T. Hadavizadeh⁵⁷, C. Hadjivasiliou⁵, G. Haefeli⁴¹, C. Haen⁴⁰, S.C. Haines⁴⁹,
 S. Hall⁵⁵, B. Hamilton⁶⁰, X. Han¹², S. Hansmann-Menzemer¹², N. Harnew⁵⁷, S.T. Harnew⁴⁸,
 J. Harrison⁵⁶, M. Hatch⁴⁰, J. He⁶³, T. Head⁴¹, A. Heister⁹, K. Hennessy⁵⁴, P. Henrard⁵,
 L. Henry⁸, J.A. Hernando Morata³⁹, E. van Herwijnen⁴⁰, M. Heß⁶⁶, A. Hicheur², D. Hill⁵⁷,
 C. Hombach⁵⁶, H. Hopchev⁴¹, W. Hulsbergen⁴³, T. Humair⁵⁵, M. Hushchyn³⁵, N. Hussain⁵⁷,
 D. Hutchcroft⁵⁴, M. Idzik²⁸, P. Ilten⁵⁸, R. Jacobsson⁴⁰, A. Jaeger¹², J. Jalocha⁵⁷, E. Jans⁴³,
 A. Jawahery⁶⁰, F. Jiang³, M. John⁵⁷, D. Johnson⁴⁰, C.R. Jones⁴⁹, C. Joram⁴⁰, B. Jost⁴⁰,
 N. Jurik⁶¹, S. Kandybei⁴⁵, W. Kanso⁶, M. Karacson⁴⁰, J.M. Kariuki⁴⁸, S. Karodia⁵³,
 M. Kecke¹², M. Kelsey⁶¹, I.R. Kenyon⁴⁷, M. Kenzie⁴⁹, T. Ketel⁴⁴, E. Khairullin³⁵,
 B. Khanji^{21,40,i}, C. Khurewathanakul⁴¹, T. Kirn⁹, S. Klaver⁵⁶, K. Klimaszewski²⁹, S. Koliiev⁴⁶,
 M. Kolpin¹², I. Komarov⁴¹, R.F. Koopman⁴⁴, P. Koppenburg⁴³, A. Kosmyntseva³²,
 A. Kozachuk³³, M. Kozeiha⁵, L. Kravchuk³⁴, K. Kreplin¹², M. Kreps⁵⁰, P. Krokovny^{36,w},
 F. Kruse¹⁰, W. Krzemien²⁹, W. Kucewicz^{27,l}, M. Kucharczyk²⁷, V. Kudryavtsev^{36,w},
 A.K. Kuonen⁴¹, K. Kurek²⁹, T. Kvaratskheliya^{32,40}, D. Lacarrere⁴⁰, G. Lafferty⁵⁶, A. Lai¹⁶,
 D. Lambert⁵², G. Lanfranchi¹⁹, C. Langenbruch⁹, T. Latham⁵⁰, C. Lazzeroni⁴⁷, R. Le Gac⁶,
 J. van Leerdam⁴³, J.-P. Lees⁴, A. Leflat^{33,40}, J. Lefrançois⁷, R. Lefèvre⁵, F. Lemaitre⁴⁰,
 E. Lemos Cid³⁹, O. Leroy⁶, T. Lesiak²⁷, B. Leverington¹², Y. Li⁷, T. Likhomanenko^{35,67},
 R. Lindner⁴⁰, C. Linn⁴⁰, F. Lionetto⁴², B. Liu¹⁶, X. Liu³, D. Loh⁵⁰, I. Longstaff⁵³, J.H. Lopes²,
 D. Lucchesi^{23,o}, M. Lucio Martinez³⁹, H. Luo⁵², A. Lupato²³, E. Luppi^{17,g}, O. Lupton⁵⁷,
 A. Lusiani²⁴, X. Lyu⁶³, F. Machefert⁷, F. Maciuc³⁰, O. Maev³¹, K. Maguire⁵⁶, S. Malde⁵⁷,
 A. Malinin⁶⁷, T. Maltsev³⁶, G. Manca⁷, G. Mancinelli⁶, P. Manning⁶¹, J. Maratas^{5,v},
 J.F. Marchand⁴, U. Marconi¹⁵, C. Marin Benito³⁸, P. Marino^{24,t}, J. Marks¹², G. Martellotti²⁶,
 M. Martin⁶, M. Martinelli⁴¹, D. Martinez Santos³⁹, F. Martinez Vidal⁶⁸, D. Martins Tostes²,
 L.M. Massacrier⁷, A. Massafferri¹, R. Matev⁴⁰, A. Mathad⁵⁰, Z. Mathe⁴⁰, C. Matteuzzi²¹,
 A. Mauri⁴², B. Maurin⁴¹, A. Mazurov⁴⁷, M. McCann⁵⁵, J. McCarthy⁴⁷, A. McNab⁵⁶,
 R. McNulty¹³, B. Meadows⁵⁹, F. Meier¹⁰, M. Meissner¹², D. Melnychuk²⁹, M. Merk⁴³,
 A. Merli^{22,q}, E. Michelin²³, D.A. Milanes⁶⁵, M.-N. Minard⁴, D.S. Mitzel¹², A. Mogini⁸,
 J. Molina Rodriguez⁶², I.A. Monroy⁶⁵, S. Monteil⁵, M. Morandin²³, P. Morawski²⁸, A. Mordà⁶,
 M.J. Morello^{24,t}, J. Moron²⁸, A.B. Morris⁵², R. Mountain⁶¹, F. Muheim⁵², M. Mulder⁴³,
 M. Mussini¹⁵, D. Müller⁵⁶, J. Müller¹⁰, K. Müller⁴², V. Müller¹⁰, P. Naik⁴⁸, T. Nakada⁴¹,
 R. Nandakumar⁵¹, A. Nandi⁵⁷, I. Nasteva², M. Needham⁵², N. Neri²², S. Neubert¹²,
 N. Neufeld⁴⁰, M. Neuner¹², A.D. Nguyen⁴¹, C. Nguyen-Mau^{41,n}, S. Nieswand⁹, R. Niet¹⁰,
 N. Nikitin³³, T. Nikodem¹², A. Novoselov³⁷, D.P. O'Hanlon⁵⁰, A. Oblakowska-Mucha²⁸,
 V. Obraztsov³⁷, S. Ogilvy¹⁹, R. Oldeman⁴⁹, C.J.G. Onderwater⁶⁹, J.M. Otalora Goicochea²,
 A. Otto⁴⁰, P. Owen⁴², A. Oyanguren⁶⁸, P.R. Pais⁴¹, A. Palano^{14,d}, F. Palombo^{22,q},
 M. Palutan¹⁹, J. Panman⁴⁰, A. Papanestis⁵¹, M. Pappagallo^{14,d}, L.L. Pappalardo^{17,g},
 W. Parker⁶⁰, C. Parkes⁵⁶, G. Passaleva¹⁸, A. Pastore^{14,d}, G.D. Patel⁵⁴, M. Patel⁵⁵,
 C. Patrignani^{15,e}, A. Pearce^{56,51}, A. Pellegrino⁴³, G. Penso²⁶, M. Pepe Altarelli⁴⁰, S. Perazzini⁴⁰,
 P. Perret⁵, L. Pescatore⁴⁷, K. Petridis⁴⁸, A. Petrolini^{20,h}, A. Petrov⁶⁷, M. Petruzzo^{22,q},
 E. Picatoste Olloqui³⁸, B. Pietrzyk⁴, M. Piekies²⁷, D. Pinci²⁶, A. Pistone²⁰, A. Piucci¹²,
 S. Playfer⁵², M. Plo Casasus³⁹, T. Poikela⁴⁰, F. Polci⁸, A. Poluektov^{50,36}, I. Polyakov⁶¹,
 E. Polcarpo², G.J. Pomery⁴⁸, A. Popov³⁷, D. Popov^{11,40}, B. Popovici³⁰, S. Poslavskii³⁷,
 C. Potterat², E. Price⁴⁸, J.D. Price⁵⁴, J. Prisciandaro³⁹, A. Pritchard⁵⁴, C. Prouve⁴⁸,
 V. Pugatch⁴⁶, A. Puig Navarro⁴¹, G. Punzi^{24,p}, W. Qian⁵⁷, R. Quagliani^{7,48}, B. Rachwal²⁷,
 J.H. Rademacker⁴⁸, M. Rama²⁴, M. Ramos Pernas³⁹, M.S. Rangel², I. Raniuk⁴⁵, G. Raven⁴⁴,
 F. Redi⁵⁵, S. Reichert¹⁰, A.C. dos Reis¹, C. Remon Alepuz⁶⁸, V. Renaudin⁷, S. Ricciardi⁵¹,
 S. Richards⁴⁸, M. Rihl⁴⁰, K. Rinnert⁵⁴, V. Rives Molina³⁸, P. Robbe^{7,40}, A.B. Rodrigues¹,
 E. Rodrigues⁵⁹, J.A. Rodriguez Lopez⁶⁵, P. Rodriguez Perez^{56,†}, A. Rogozhnikov³⁵, S. Roiser⁴⁰,
 A. Rollings⁵⁷, V. Romanovskiy³⁷, A. Romero Vidal³⁹, J.W. Ronayne¹³, M. Rotondo¹⁹,
 M.S. Rudolph⁶¹, T. Ruf⁴⁰, P. Ruiz Valls⁶⁸, J.J. Saborido Silva³⁹, E. Sadykhov³², N. Sagidova³¹,

B. Saitta^{16,f}, V. Salustino Guimaraes², C. Sanchez Mayordomo⁶⁸, B. Sanmartin Sedes³⁹, R. Santacesaria²⁶, C. Santamarina Rios³⁹, M. Santimaria¹⁹, E. Santovetti^{25,j}, A. Sarti^{19,k}, C. Satriano^{26,s}, A. Satta²⁵, D.M. Saunders⁴⁸, D. Savrina^{32,33}, S. Schael⁹, M. Schellenberg¹⁰, M. Schiller⁴⁰, H. Schindler⁴⁰, M. Schlupp¹⁰, M. Schmelling¹¹, T. Schmelzer¹⁰, B. Schmidt⁴⁰, O. Schneider⁴¹, A. Schopper⁴⁰, K. Schubert¹⁰, M. Schubiger⁴¹, M.-H. Schune⁷, R. Schwemmer⁴⁰, B. Sciascia¹⁹, A. Sciubba^{26,k}, A. Semennikov³², A. Sergi⁴⁷, N. Serra⁴², J. Serrano⁶, L. Sestini²³, P. Seyfert²¹, M. Shapkin³⁷, I. Shapoval⁴⁵, Y. Shcheglov³¹, T. Shears⁵⁴, L. Shekhtman^{36,w}, V. Shevchenko⁶⁷, A. Shires¹⁰, B.G. Siddi^{17,40}, R. Silva Coutinho⁴², L. Silva de Oliveira², G. Simi^{23,o}, S. Simone^{14,d}, M. Sirendi⁴⁹, N. Skidmore⁴⁸, T. Skwarnicki⁶¹, E. Smith⁵⁵, I.T. Smith⁵², J. Smith⁴⁹, M. Smith⁵⁵, H. Snoek⁴³, M.D. Sokoloff⁵⁹, F.J.P. Soler⁵³, B. Souza De Paula², B. Spaan¹⁰, P. Spradlin⁵³, S. Sridharan⁴⁰, F. Stagni⁴⁰, M. Stahl¹², S. Stahl⁴⁰, P. Stefko⁴¹, S. Stefkova⁵⁵, O. Steinkamp⁴², S. Stemmler¹², O. Stenyakin³⁷, S. Stevenson⁵⁷, S. Stoica³⁰, S. Stone⁶¹, B. Storaci⁴², S. Stracka^{24,p}, M. Straticiu³⁰, U. Straumann⁴², L. Sun⁵⁹, W. Sutcliffe⁵⁵, K. Swientek²⁸, V. Syropoulos⁴⁴, M. Szczekowski²⁹, T. Szumlak²⁸, S. T'Jampens⁴, A. Tayduganov⁶, T. Tekampe¹⁰, M. Teklishyn⁷, G. Tellarini^{17,g}, F. Teubert⁴⁰, E. Thomas⁴⁰, J. van Tilburg⁴³, M.J. Tilley⁵⁵, V. Tisserand⁴, M. Tobin⁴¹, S. Tolk⁴⁹, L. Tomassetti^{17,g}, D. Tonelli⁴⁰, S. Topp-Joergensen⁵⁷, F. Toriello⁶¹, E. Tournefier⁴, S. Tourneur⁴¹, K. Trabelsi⁴¹, M. Traill⁵³, M.T. Tran⁴¹, M. Tresch⁴², A. Trisovic⁴⁰, A. Tsaregorodtsev⁶, P. Tsopelas⁴³, A. Tully⁴⁹, N. Tuning⁴³, A. Ukleja²⁹, A. Ustyuzhanin³⁵, U. Uwer¹², C. Vacca^{16,f}, V. Vagnoni^{15,40}, A. Valassi⁴⁰, S. Valat⁴⁰, G. Valenti¹⁵, A. Vallier⁷, R. Vazquez Gomez¹⁹, P. Vazquez Regueiro³⁹, S. Vecchi¹⁷, M. van Veghel⁴³, J.J. Velthuis⁴⁸, M. Veltri^{18,r}, G. Veneziano⁴¹, A. Venkateswaran⁶¹, M. Vernet⁵, M. Vesterinen¹², B. Viaud⁷, D. Vieira¹, M. Vieites Diaz³⁹, X. Vilasis-Cardona^{38,m}, V. Volkov³³, A. Vollhardt⁴², B. Voneki⁴⁰, A. Vorobyev³¹, V. Vorobyev^{36,w}, C. Voß⁶⁶, J.A. de Vries⁴³, C. Vázquez Sierra³⁹, R. Waldi⁶⁶, C. Wallace⁵⁰, R. Wallace¹³, J. Walsh²⁴, J. Wang⁶¹, D.R. Ward⁴⁹, H.M. Wark⁵⁴, N.K. Watson⁴⁷, D. Websdale⁵⁵, A. Weiden⁴², M. Whitehead⁴⁰, J. Wicht⁵⁰, G. Wilkinson^{57,40}, M. Wilkinson⁶¹, M. Williams⁴⁰, M.P. Williams⁴⁷, M. Williams⁵⁸, T. Williams⁴⁷, F.F. Wilson⁵¹, J. Wimberley⁶⁰, J. Wishahi¹⁰, W. Wislicki²⁹, M. Witek²⁷, G. Wormser⁷, S.A. Wotton⁴⁹, K. Wraight⁵³, S. Wright⁴⁹, K. Wyllie⁴⁰, Y. Xie⁶⁴, Z. Xing⁶¹, Z. Xu⁴¹, Z. Yang³, H. Yin⁶⁴, J. Yu⁶⁴, X. Yuan^{36,w}, O. Yushchenko³⁷, K.A. Zarebski⁴⁷, M. Zavertyaev^{11,c}, L. Zhang³, Y. Zhang⁷, Y. Zhang⁶³, A. Zhelezov¹², Y. Zheng⁶³, A. Zhokhov³², X. Zhu³, V. Zhukov⁹, S. Zucchelli¹⁵.

¹Centro Brasileiro de Pesquisas Físicas (CBPF), Rio de Janeiro, Brazil

²Universidade Federal do Rio de Janeiro (UFRJ), Rio de Janeiro, Brazil

³Center for High Energy Physics, Tsinghua University, Beijing, China

⁴LAPP, Université Savoie Mont-Blanc, CNRS/IN2P3, Annecy-Le-Vieux, France

⁵Clermont Université, Université Blaise Pascal, CNRS/IN2P3, LPC, Clermont-Ferrand, France

⁶CPPM, Aix-Marseille Université, CNRS/IN2P3, Marseille, France

⁷LAL, Université Paris-Sud, CNRS/IN2P3, Orsay, France

⁸LPNHE, Université Pierre et Marie Curie, Université Paris Diderot, CNRS/IN2P3, Paris, France

⁹I. Physikalisches Institut, RWTH Aachen University, Aachen, Germany

¹⁰Fakultät Physik, Technische Universität Dortmund, Dortmund, Germany

¹¹Max-Planck-Institut für Kernphysik (MPIK), Heidelberg, Germany

¹²Physikalisches Institut, Ruprecht-Karls-Universität Heidelberg, Heidelberg, Germany

¹³School of Physics, University College Dublin, Dublin, Ireland

¹⁴Sezione INFN di Bari, Bari, Italy

¹⁵Sezione INFN di Bologna, Bologna, Italy

¹⁶Sezione INFN di Cagliari, Cagliari, Italy

¹⁷Sezione INFN di Ferrara, Ferrara, Italy

¹⁸Sezione INFN di Firenze, Firenze, Italy

¹⁹Laboratori Nazionali dell'INFN di Frascati, Frascati, Italy

²⁰Sezione INFN di Genova, Genova, Italy

²¹Sezione INFN di Milano Bicocca, Milano, Italy

- ²² *Sezione INFN di Milano, Milano, Italy*
- ²³ *Sezione INFN di Padova, Padova, Italy*
- ²⁴ *Sezione INFN di Pisa, Pisa, Italy*
- ²⁵ *Sezione INFN di Roma Tor Vergata, Roma, Italy*
- ²⁶ *Sezione INFN di Roma La Sapienza, Roma, Italy*
- ²⁷ *Henryk Niewodniczanski Institute of Nuclear Physics Polish Academy of Sciences, Kraków, Poland*
- ²⁸ *AGH - University of Science and Technology, Faculty of Physics and Applied Computer Science, Kraków, Poland*
- ²⁹ *National Center for Nuclear Research (NCBJ), Warsaw, Poland*
- ³⁰ *Horia Hulubei National Institute of Physics and Nuclear Engineering, Bucharest-Magurele, Romania*
- ³¹ *Petersburg Nuclear Physics Institute (PNPI), Gatchina, Russia*
- ³² *Institute of Theoretical and Experimental Physics (ITEP), Moscow, Russia*
- ³³ *Institute of Nuclear Physics, Moscow State University (SINP MSU), Moscow, Russia*
- ³⁴ *Institute for Nuclear Research of the Russian Academy of Sciences (INR RAN), Moscow, Russia*
- ³⁵ *Yandex School of Data Analysis, Moscow, Russia*
- ³⁶ *Budker Institute of Nuclear Physics (SB RAS), Novosibirsk, Russia*
- ³⁷ *Institute for High Energy Physics (IHEP), Protvino, Russia*
- ³⁸ *ICCUB, Universitat de Barcelona, Barcelona, Spain*
- ³⁹ *Universidad de Santiago de Compostela, Santiago de Compostela, Spain*
- ⁴⁰ *European Organization for Nuclear Research (CERN), Geneva, Switzerland*
- ⁴¹ *Ecole Polytechnique Fédérale de Lausanne (EPFL), Lausanne, Switzerland*
- ⁴² *Physik-Institut, Universität Zürich, Zürich, Switzerland*
- ⁴³ *Nikhef National Institute for Subatomic Physics, Amsterdam, The Netherlands*
- ⁴⁴ *Nikhef National Institute for Subatomic Physics and VU University Amsterdam, Amsterdam, The Netherlands*
- ⁴⁵ *NSC Kharkiv Institute of Physics and Technology (NSC KIPT), Kharkiv, Ukraine*
- ⁴⁶ *Institute for Nuclear Research of the National Academy of Sciences (KINR), Kyiv, Ukraine*
- ⁴⁷ *University of Birmingham, Birmingham, United Kingdom*
- ⁴⁸ *H.H. Wills Physics Laboratory, University of Bristol, Bristol, United Kingdom*
- ⁴⁹ *Cavendish Laboratory, University of Cambridge, Cambridge, United Kingdom*
- ⁵⁰ *Department of Physics, University of Warwick, Coventry, United Kingdom*
- ⁵¹ *STFC Rutherford Appleton Laboratory, Didcot, United Kingdom*
- ⁵² *School of Physics and Astronomy, University of Edinburgh, Edinburgh, United Kingdom*
- ⁵³ *School of Physics and Astronomy, University of Glasgow, Glasgow, United Kingdom*
- ⁵⁴ *Oliver Lodge Laboratory, University of Liverpool, Liverpool, United Kingdom*
- ⁵⁵ *Imperial College London, London, United Kingdom*
- ⁵⁶ *School of Physics and Astronomy, University of Manchester, Manchester, United Kingdom*
- ⁵⁷ *Department of Physics, University of Oxford, Oxford, United Kingdom*
- ⁵⁸ *Massachusetts Institute of Technology, Cambridge, MA, United States*
- ⁵⁹ *University of Cincinnati, Cincinnati, OH, United States*
- ⁶⁰ *University of Maryland, College Park, MD, United States*
- ⁶¹ *Syracuse University, Syracuse, NY, United States*
- ⁶² *Pontifícia Universidade Católica do Rio de Janeiro (PUC-Rio), Rio de Janeiro, Brazil, associated to ²*
- ⁶³ *University of Chinese Academy of Sciences, Beijing, China, associated to ³*
- ⁶⁴ *Institute of Particle Physics, Central China Normal University, Wuhan, Hubei, China, associated to ³*
- ⁶⁵ *Departamento de Física, Universidad Nacional de Colombia, Bogota, Colombia, associated to ⁸*
- ⁶⁶ *Institut für Physik, Universität Rostock, Rostock, Germany, associated to ¹²*
- ⁶⁷ *National Research Centre Kurchatov Institute, Moscow, Russia, associated to ³²*
- ⁶⁸ *Instituto de Física Corpuscular (IFIC), Universitat de Valencia-CSIC, Valencia, Spain, associated to ³⁸*
- ⁶⁹ *Van Swinderen Institute, University of Groningen, Groningen, The Netherlands, associated to ⁴³*
- ^a *Universidade Federal do Triângulo Mineiro (UFTM), Uberaba-MG, Brazil*
- ^b *Laboratoire Leprince-Ringuet, Palaiseau, France*
- ^c *P.N. Lebedev Physical Institute, Russian Academy of Science (LPI RAS), Moscow, Russia*
- ^d *Università di Bari, Bari, Italy*
- ^e *Università di Bologna, Bologna, Italy*
- ^f *Università di Cagliari, Cagliari, Italy*

- ^g *Università di Ferrara, Ferrara, Italy*
^h *Università di Genova, Genova, Italy*
ⁱ *Università di Milano Bicocca, Milano, Italy*
^j *Università di Roma Tor Vergata, Roma, Italy*
^k *Università di Roma La Sapienza, Roma, Italy*
^l *AGH - University of Science and Technology, Faculty of Computer Science, Electronics and Telecommunications, Kraków, Poland*
^m *LIFAEELS, La Salle, Universitat Ramon Llull, Barcelona, Spain*
ⁿ *Hanoi University of Science, Hanoi, Viet Nam*
^o *Università di Padova, Padova, Italy*
^p *Università di Pisa, Pisa, Italy*
^q *Università degli Studi di Milano, Milano, Italy*
^r *Università di Urbino, Urbino, Italy*
^s *Università della Basilicata, Potenza, Italy*
^t *Scuola Normale Superiore, Pisa, Italy*
^u *Università di Modena e Reggio Emilia, Modena, Italy*
^v *Iligan Institute of Technology (IIT), Iligan, Philippines*
^w *Novosibirsk State University, Novosibirsk, Russia*

[†] *Deceased*